Hindawi
Advances in Civil Engineering
Volume 2019, Article ID 6857683, 14 pages
https://doi.org/10.1155/2019/6857683

Research Article

Experimental Research and Theoretical Analysis of the Seismic Behavior of Prefabricated Semirigid Steel Frame with X-Shaped Braces

Rongqian Yang[1] **and Xuejun Zhou**[2]

[1]*School of Civil Engineering, Shandong University, Ji'nan, China*
[2]*School of Civil Engineering, Shandong Jianzhu University, Ji'nan, China*

Correspondence should be addressed to Xuejun Zhou; xuejunzhou@sdjzu.edu.cn

Received 20 March 2019; Revised 18 July 2019; Accepted 30 July 2019; Published 29 August 2019

Academic Editor: Antonio Formisano

Copyright © 2019 Rongqian Yang and Xuejun Zhou. This is an open access article distributed under the Creative Commons Attribution License, which permits unrestricted use, distribution, and reproduction in any medium, provided the original work is properly cited.

Three semirigid connections which are convenient for prefabrication have been proposed in this paper. Based on them, the quasi-static test was conducted on three prefabricated semirigid steel frames with X-shaped braces in order to investigate their hysteresis behavior, bearing capacity, energy dissipation capacity, and failure mechanism. A comparative analysis of the semirigid connections was made to analyze their advantages and disadvantages. Then, a numerical simulation was carried out via using ABAQUS to verify the test results, and the causes of the errors were analyzed. The results showed that the prefabricated semirigid steel frames with X-shaped braces had good seismic behavior, the braces cooperated well with the steel frame in resisting lateral load, and the braces failed before the steel frame, which meant the structure had two seismic fortification lines. The results of the numerical simulation tallied with the test results, which means the finite element model could accurately simulate the structure's mechanical behavior under cyclic loading. The structure had a better bearing capacity and ductility when using extended end-plate bolted connections.

1. Introduction

Vigorously promoting and developing steel structure buildings can not only relieve the excess capacity of steel industry but also promote the greening, industrialization, and informationization of buildings, thus realizing the transformation and upgradation of traditional industries [1]. The development of steel structure houses is the key to promoting the application of steel structures [2]. Steel structure houses usually adopt a frame structure. Currently, the connections between beams and columns are all bolt-weld mixed, which does not meet the requirements of building industrialization. Therefore, it is necessary to study the connections of nonwelding.

At present, the connections between beams and columns in steel frames all adopt either rigid connections or hinged connections. However, due to the limited stiffness of the connections used in actual engineering, it is difficult to form an ideal rigid or hinged connection, so a semirigid connection objectively exists [3]. Previous studies [4–18] have shown that a semirigid connection will prolong the natural vibration period, increase damping, and increase the energy dissipation capacity but will also decrease the structural stiffness and enlarge the lateral displacement. Under a rare earthquake, the braces in a concentrically braced steel frame system, acting as the first seismic fortification line, appear to be unstable, yielding or even failing the before steel frame, while the frame acts as the second seismic fortification line [19–25]. The design concept of two seismic fortification lines is in line with the modern aseismic design concept. Therefore, this type of structure has been widely used in multistory steel-structure buildings [26, 27]. By combining the X-shaped concentrically braced frame with the semirigid steel frame, it is possible to form a prefabricated semirigid

steel frame with X-shaped concentric braces. The braces can compensate for the weakness of lateral stiffness in the semirigid steel frame and produce a satisfactory ductility and energy dissipation capacity, which shows promise for use in engineering applications.

Based on engineering practice, three semirigid steel frame specimens with X-shaped braces and different prefabricated semirigid connections was designed, and quasi-static tests were performed on the specimens. The loading process, working mechanism, hysteretic behavior, energy dissipation capacity, and ductility were analyzed. Combined with the results of the low-cycle reciprocating test and considering the Bauschinger effect of the material, ABAQUS software was used to conduct a nonlinear numerical simulation on the specimens. The simulation results were then compared with the experimental results to explain the cause of the errors.

2. Test Overview

2.1. Specimen Overview

2.1.1. Design of the Specimen. The specimen tested was a single frame with two spans and two floors, with a scale ratio of 1 : 2. One of the spans was an X-shaped concentrically braced frame. The other span was a semirigid bending-resistant steel frame. The beams and columns of the two spans had the same cross section. The axis distance was $3000 \times 2 = 6000$ mm, and the total height was 3117 mm, as shown in Figure 1. The semirigid connections were in the form of top-seat angle connections with web and ear plates, extended end-plate bolted connections, and T-section connections. The three forms of connections are shown in Figure 2. The braces were connected to the steel frame by a gusset plate. The cross-sectional dimensions of the components are presented in Table 1. The specimen numbers are presented in Table 2.

The tested frames were designed by finite element analysis software SAP2000. In order to acquire the proper scantling, the Pushover analysis was conducted and the displacement control method was adopted. According to the Code for Seismic Design of Buildings [28], the story angle limitation was determined as 1/250 under the frequent earthquake and 1/50 under the rare earthquake. The semirigid connections were simulated by nonlinear connection element with Takeda plastic property. The nonlinear influence should be considered in the Pushover analysis. The P-Δ effect and plastic hinge could separately achieve the geometric nonlinearity and material nonlinearity. The results showed that the plastic hinges on the frames followed the appearance sequence of "brace-beam-column" and the max displacement did not reach the limitation, which indicated the frames had reasonable design and could be studied in the following tests.

2.1.2. Material Test. All of the specimens were made from Q235B steel. The yield strength f_y, the ultimate tensile strength f_u, the modulus of elasticity E, and the elongation δ of the steel were determined by the material tests. The material tests were conducted according to the relevant provisions of the National Standards Metallic Materials—Tensile Testing—Part 1: Method of Test at Room Temperature [29] and Steel and Steel Products—Location and Preparation of Test Pieces for Mechanical Testing [30]. The results are shown in Table 3.

2.1.3. Test Equipment. According to the Specification for seismic test of buildings [31], the test uses a dual control load-deformation method. Before the specimen yields, load control should adopt step loading. After the specimen yields, deformation control should be adopted, where the deformation value uses the maximum displacement value when yielded, and the loading is performed in steps by a multiple of the displacement value. Each stage of the load is cycled twice.

In the test, a constant vertical load was first applied to the top of the column, and then a horizontal low-cycle reciprocating load was applied at the end of the top-floor beam. The vertical load was provided by three 30 t hydraulic jacks. One end of the Jack was connected to the top of the column, and the other end was fixed to the girder of the loading portal. A roller device was arranged between the Jack and the girder to enable the Jack to maintain real-time horizontal movement with the top of the column and to reduce the effects of friction. The horizontal reciprocating load was provided by a 100 t MTS electro-hydraulic servo actuator. One end of the actuator was fixed to the reaction wall, and the other end was connected to the specimen. The actuator had a stroke of ±250 mm. In order to ensure the out-of-plane stability of the specimen during the test, lateral braces of sufficient stiffness were installed at the connections of the first and second-floor as well as the middle of the beams. Rollers were installed on the lateral braces to reduce the influence of friction on the in-plane horizontal load. The column base and the ground beam were welded together to achieve the boundary condition of fixed-end constraint. The test setup is shown in Figure 3.

To measure the lateral deformation, displacement meters are set at the first and second levels of the beam center line, as shown in Figure 4. In addition, one-way strain gauge and tridirectional strain rosette are arranged in critical stress positions such as the column base, brace and beam end to measure the change of internal force, which is presented in Figure 5.

2.2. Test Phenomena. The test phenomena of the specimens were generally the same, with only minor differences. Considering the limited space in this paper, a representative specimen C-JB was selected to elaborate the test phenomena.

It can be seen from Table 4 and Figure 6 that the brace damage of the C-JB specimen mainly occurred at the connection. This is because the connection was in a multidirectional stress state under the reciprocating load, and the section's plasticity was not easy to develop, showing characteristics of brittle fracture. After removal of the load, the deformation of the steel beam without the braced span was basically restored, and the deformation of the column base

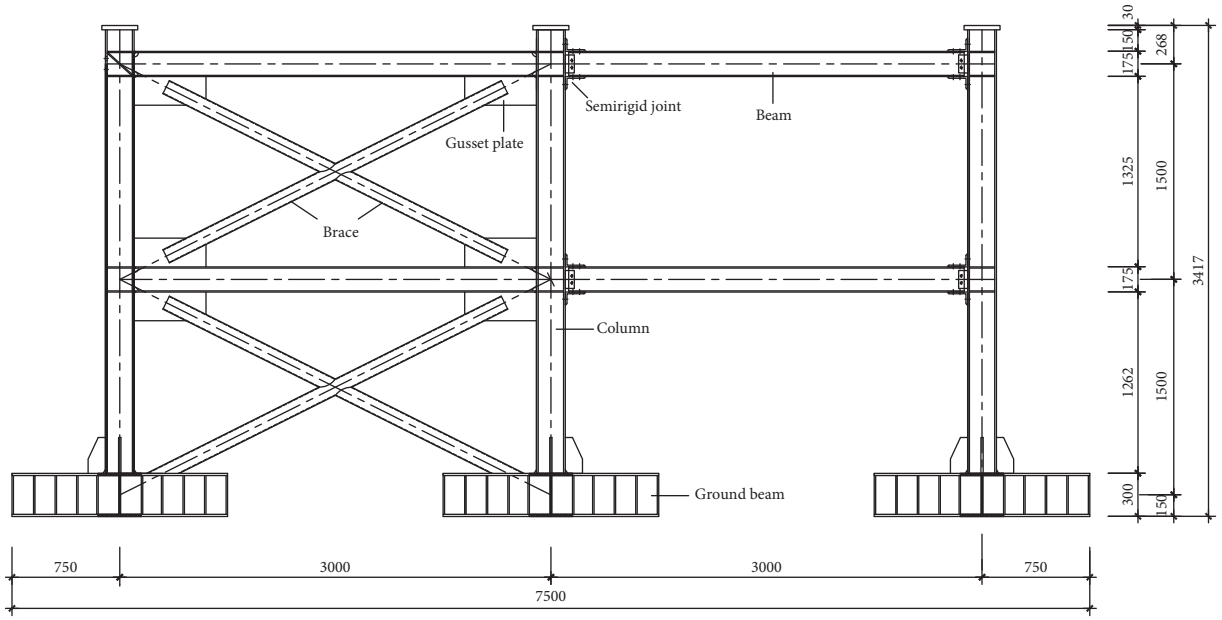

Figure 1: Dimensions of the specimens.

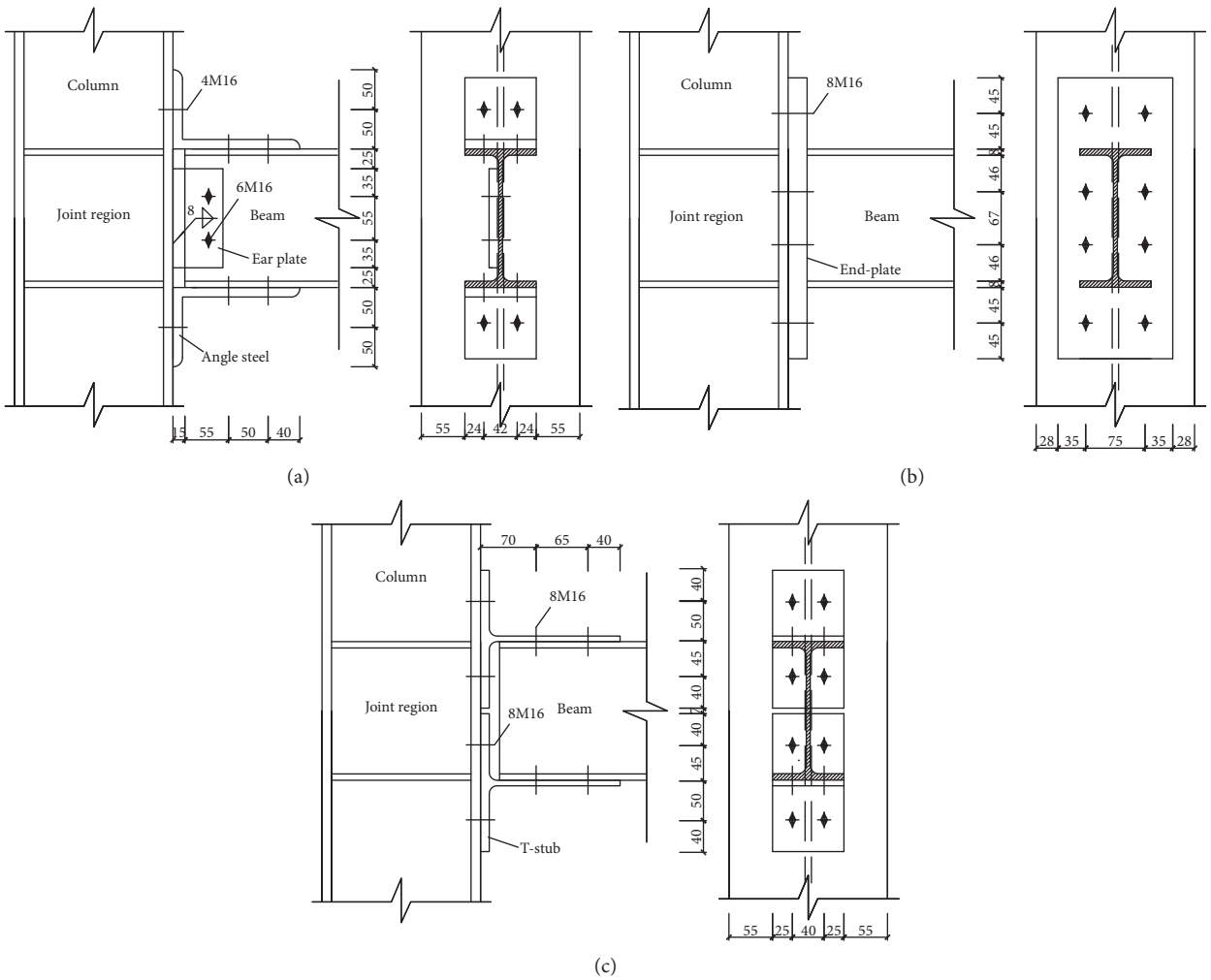

Figure 2: Forms of the semirigid connections. (a) J-1: top-seat angle connection with web and ear plates. (b) J-2: extended end-plate connection. (c) J-3: T-section connection.

Table 1: Specification of the specimens (unit: mm).

Component	Dimensions of the cross section
Frame column	HW200 × 200 × 8 × 12
Frame beam	HN175 × 90 × 5 × 8
Brace	Φ76 × 4
Ground beam	HW300 × 300 × 8 × 12

Table 2: Number of specimens.

Sequence	Name	Connection form
1	C-JA	Top-seat angle connection with web and ear plates
2	C-JB	Extended end-plate connection
3	C-JC	T-section connection

was not obvious, but the strain data showed that the column base had been plastically developed.

The steel beam with the braced span and the brace retained a large residual deformation, and the semirigid connection displayed no obvious deformation. It can be seen from the whole test process that the structure generally followed the failure sequence of "brace-beam-column" and had two seismic fortification lines. The structure could follow the design principles of "strong column—weak beam" and "strong connection—weak component" as well as the design criteria of "elastic deformation in a small earthquake; no yielding of braces and elastic deformation of the frame in a moderate earthquake; allowable breaking of braces and no yielding of the frame in a large earthquake."

2.3. Data Analysis

2.3.1. Hysteresis Curve. Taking the lateral displacement value of the top floor as the abscissa and the horizontal load applied by the actuator as the ordinate, the hysteresis curve for each specimen could be plotted, as shown in Figure 5.

The hysteresis curves reflect the trend of the energy dissipation capacity, load-bearing capacity and lateral stiffness of the structure. It can be seen from Figure 7 that during the whole loading process, the hysteresis curves presented a "three-stage form," that is, the hysteresis curve could be divided into three stages according to the diagonal slope of the hysteresis loop. Firstly, in the initial stage, the hysteresis curves were approximately linear, and there was almost no residual deformation after unloading, the specimens displayed no energy dissipation. In this stage, the specimen remained in the elastic state, with the largest diagonal slope, and the lateral stiffness was provided by the braces and the semirigid steel frame. Secondly, as the lateral displacement increased, the braces displayed elastic-plastic deformation and it was expanded continuously. The hysteresis curves began to appear nonlinear, and the area enclosed by the hysteresis loop increased, forming a full shuttle shape. The energy dissipation of the specimens gradually increased and the diagonal slope of the hysteresis loop gradually decreased, which indicates that the overall lateral stiffness of the specimens was degraded continuously. Thirdly, in the final stage, the braces basically did not function and the diagonal slope of the hysteresis loop was the smallest. The lateral stiffness was only provided by the semirigid steel frame, but the hysteresis loop still formed a full shuttle shape and had no obvious slippage. The load-bearing capacity of the steel frame was not significantly reduced, indicating that the semirigid steel frame had a good load-bearing capacity and stable energy dissipation performance.

Through comparison of the hysteresis curves, it can be seen that in the elastic stage, the hysteresis curves of the specimens were not much different, and the initial stiffness was very similar. In the elastic-plastic stage, the interfloor displacement angle of each specimen was about 1/268, lower than 1/250. The maximum elastic-plastic deformation of specimens C-JA, C-JB and C-JC were 39.2 mm, 44.8 mm and 42.0 mm respectively, and the corresponding elastic-plastic interfloor displacement angles were 1/77, 1/67 and 1/71 respectively, all lower than 1/50, meeting the requirements of the specification. At the same time, it can be seen that the curve of specimen C-JB was the smoothest, with no sudden change in load-bearing capacity or deformation ability, followed by specimens C-JC and C-JA. In the final stage of loading, the diagonal slope of the hysteresis curve of each specimen was almost the same, and the lateral stiffness of the semirigid steel frame was similar. However, the load-bearing capacity of the C-JB semirigid steel frame was about 12% higher than the other two, displaying a better load bearing capacity.

2.3.2. Skeleton Curve. The skeleton curves of the specimens are shown in Figure 8. It can be seen from Figure 8 that the skeleton curves had good symmetry for both positive and negative displacements and the initial elastic stiffness was basically the same. The skeleton curves have an inverted S-shape, which indicated that the stress process could be roughly divided into three stages: the elastic stage, plastic stage and failure stage.

In the initial loading stage, the horizontal load and displacement increased linearly, indicating that the specimen was in the elastic stage. After the elastic stage, the skeleton curve appeared nonlinear, and the slope of the curve decreased, indicating that the stiffness was degraded and the specimen entered the elastic-plastic stage because the braces developed a crack at the cross connection of the X-shaped brace, further resulting in a gradual decrease in the lateral stiffness of the specimen.

All the specimens then reached a peak load at $\delta = \pm 16.8$ mm. When the specimens reached a displacement of $\delta = \pm 22.4$ mm, the skeleton curve displayed a more obvious turning point, and the horizontal load dropped sharply. This was because the brace had broken and the specimen experienced a sudden change in stiffness, which was brittle failure. However, because the specimen still possessed a high lateral stiffness, the internal force was redistributed, and the load bearing capacity continued to grow slowly. As the load increased, the failure of the brace was intensified, and the skeleton curve displayed a slowly

Table 3: Result of tensile coupon test.

Number		Thickness (mm)		f_y (N/mm^2)	f_u (N/mm^2)	E, 10^5 (N/mm^2)	Elongation (%)
		Nominal	Measured				
S1	S1-1	10	9.84	230	405	2.09	31.4
	S1-2	10	9.74	235	405	2.07	31.2
	S1-3	10	9.72	225	395	2.04	31.5
	Average	10	9.77	230	401.7	2.07	31.4

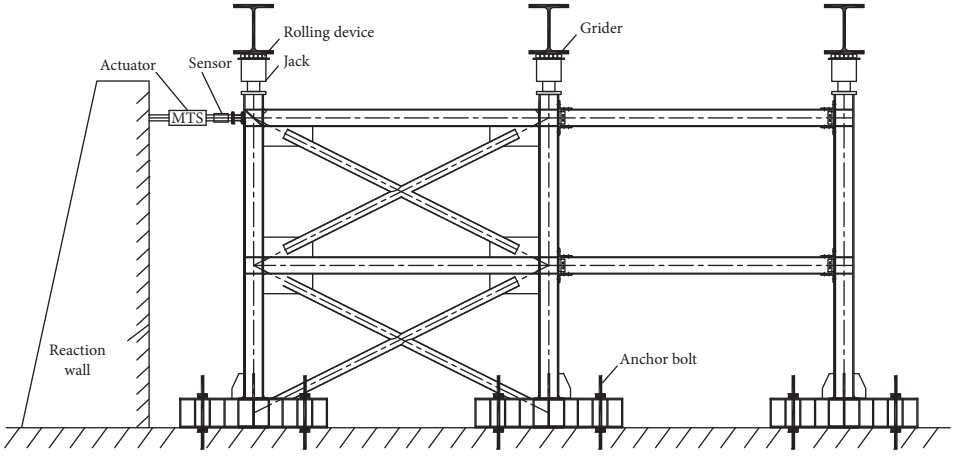

(a)

(b)

Figure 3: Test setup. (a) Schematic of the test setup. (b) Actual test setup.

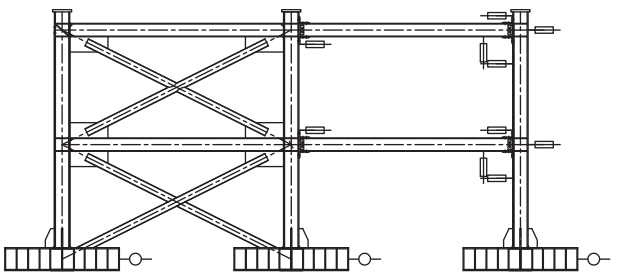

Figure 4: Measurement of displacement.

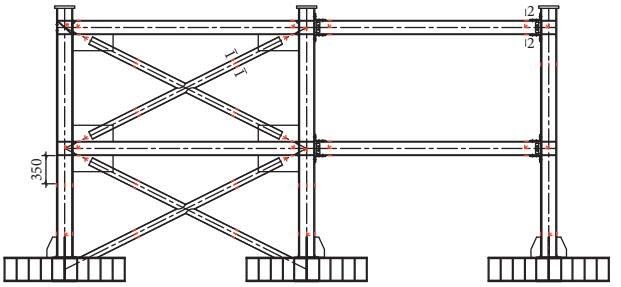

Figure 5: Measurement of strain.

Table 4: Test phenomena.

Specimen	Loading stage	Test phenomena
C-JB	Elastic stage	No obvious phenomenon
	$1.5\Delta_y$	The component was slightly audible
	$2\Delta_y$	The steel pipe wall of the X-shaped connection at the floor-two brace was subjected to compressive deformation and tensile tearing, see Figures 6(a) and 6(b)
	$3\Delta_y$	The crack of the X-shaped connection at the floor-two brace expanded and broke, see Figures 6(c) and 6(d)
	$4\Delta_y$	Slight out of plane buckling at the floor-two beam end
	$5\Delta_y$	Crack occurred at the steel pipe wall of the X-shaped connection at the floor-one brace, see Figure 6(e)
	$6\Delta_y$	The crack at the connection expanded, and the out of plane buckling of the floor-one beam intensified.
	$7\Delta_y$	The crack at the connection further expanded and the failure was serious, see Figure 6(f)
	$8\Delta_y$	The floor-one brace broke at the connection, see Figure 6(g)
	$9\Delta_y$	The floor-two beam had serious out of plane buckling, see Figure 6(h)
	$10\Delta_y$	Side column twisted

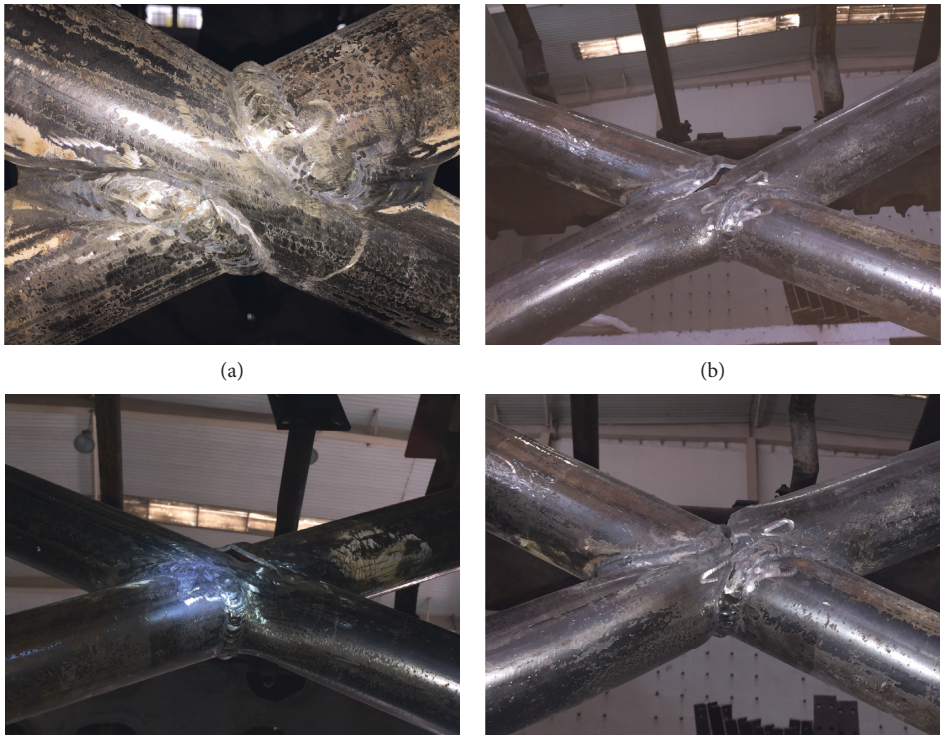

(a) (b) (c) (d)

Figure 6: Continued.

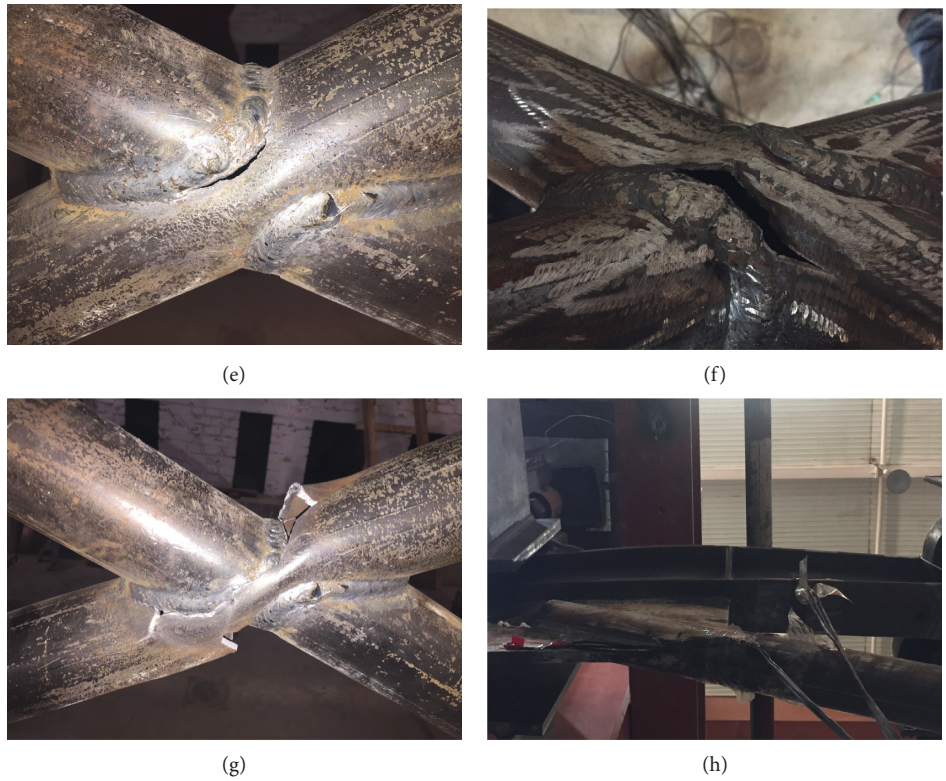

Figure 6: Failure phenomenon of the specimen C-JB. (a) Deformation of the connection. (b) Crack of the connection of the floor-two brace. (c) Crack of the brace expanded. (d) Floor-two brace broke. (e) Crack of the connection at the floor-one brace. (f) Serious damage of the brace. (g) Floor-one braces broke. (h) Out of plane buckling of the floor-two beam.

falling trend, meaning the specimen entered the failure stage. In the failure stage, the brace basically did not function, and only the semirigid steel frame was stressed. The curve displayed a slow downward trend, indicating that the semirigid steel frame also had good ductility and load-bearing capacity.

Comparing the skeleton curves, the ultimate displacement for each specimen was the same, and the peak load of specimen C-JC was the largest, which was 6.4% and 12.6% higher than that of specimens C-JB and C-JA, respectively; in the final stage of loading, specimen C-JB had the highest load bearing capacity, which was 35.8% and 21.9% higher than specimens C-JA and C-JC, respectively. It can be seen that the ductility of specimen C-JB was the best.

2.3.3. Energy Dissipation Performance. Energy dissipation is one of the main indicators when evaluating the seismic performance of a structure. Under the action of a low-cycle reciprocating load, the area of the hysteresis loop represents the energy dissipation capacity of the structure. The fuller the hysteresis loop, the better the energy dissipation performance. Based on the experimental data, the accumulated energy dissipation in each loading cycle can be found. The energy dissipation capacity can be expressed by the energy dissipation coefficient E. A larger energy dissipation coefficient indicates a better energy dissipation performance and a better seismic performance. The energy dissipation coefficient E can be calculated by

$$E = \frac{S_{(\mathrm{ABC+CDA})}}{S_{(\mathrm{OBE+ODF})}}, \tag{1}$$

where $S_{(\mathrm{ABC+CDA})}$ represents the area enclosed by the hysteresis loop; $S_{(\mathrm{OBE+ODF})}$ represents the area enclosed by the corresponding triangle, as shown in Figure 9.

The variation of the energy dissipation coefficient of each specimen in the loading process is shown in Figure 10. It can be seen that in the initial loading stage, the energy dissipation coefficient was small, indicating that the structure was in the elastic stage, and there was almost no energy dissipation. After entering the elastic-plastic stage, the brace dissipated the energy and the coefficient increased remarkably. As the loading continued, the damage to the brace accumulated and the energy dissipation coefficient tended to be stable. In the final loading stage, the brace basically did not function, and only the semirigid steel frame absorbed energy, which led to the energy dissipation coefficient decrease.

The energy dissipation coefficients of the specimens C-JA, C-JB and C-JC were all small in the elastic-plastic stage. This is because the intersecting connections were in a multi-directional complex stress state under the reciprocating load, so that a crack was generated prematurely, the plasticity of the brace was not fully developed, and the energy dissipation capacity was not fully utilized either.

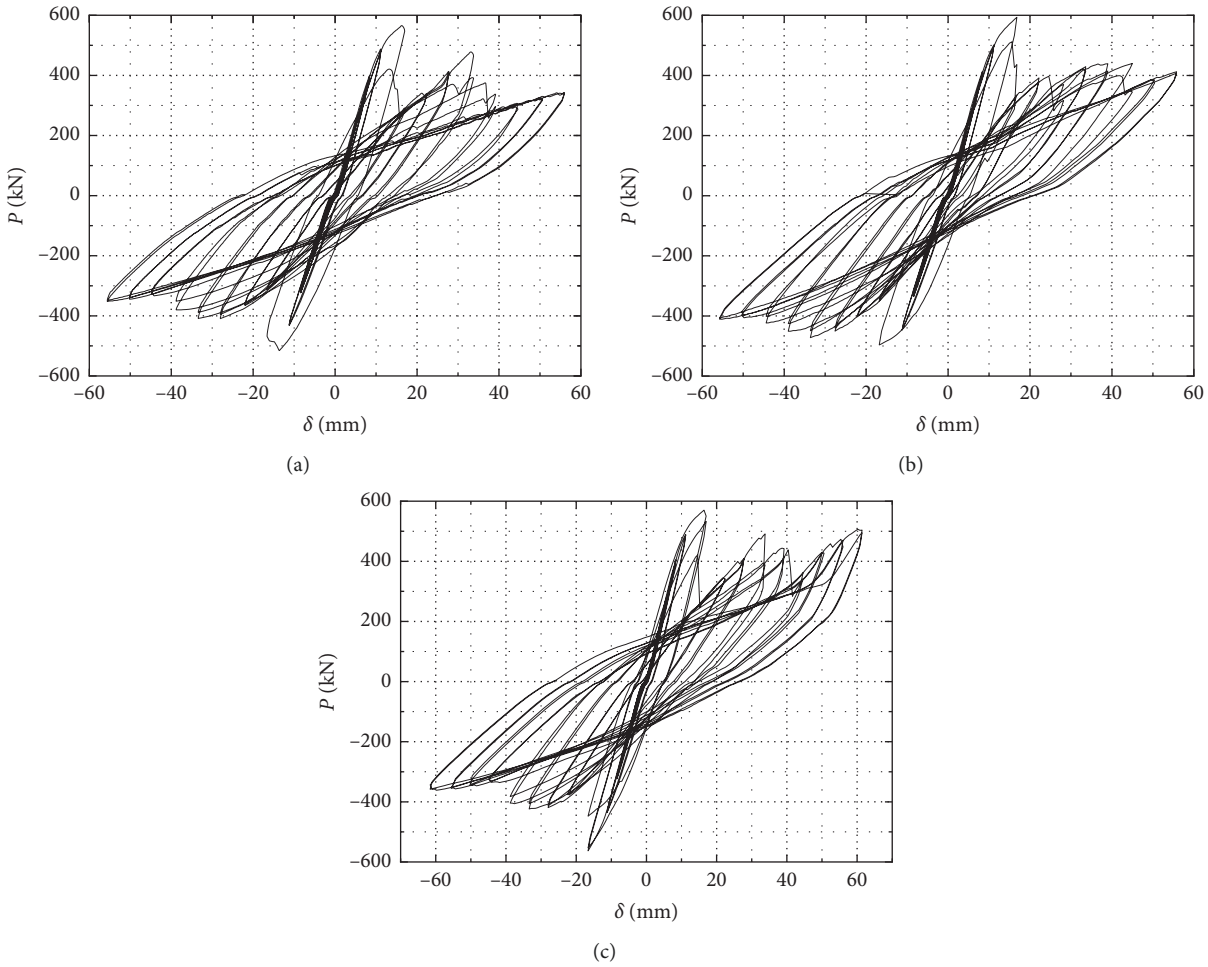

Figure 7: Hysteresis curves of the specimens. (a) Hysteresis curve of the specimen C-JA. (b) Hysteresis curve of the specimen C-JB. (c) Hysteresis curve of the specimen C-JC.

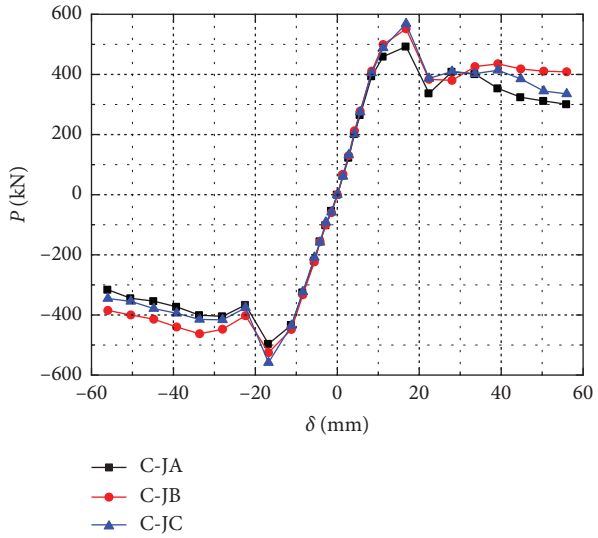

Figure 8: Skeleton curve of the specimens.

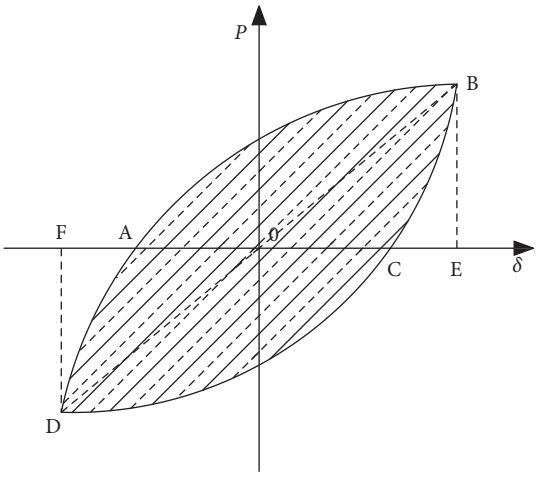

Figure 9: Load-displacement curve.

Comparing the specimens, it can be seen that in the final stage of loading, the energy dissipation coefficient of the specimen C-JA was the highest, followed by the specimens C-JB and C-JC. The variation law is opposite to the bearing capacity, and is inversely proportional to the relative magnitude of the semirigid connection's initial rotational stiffness.

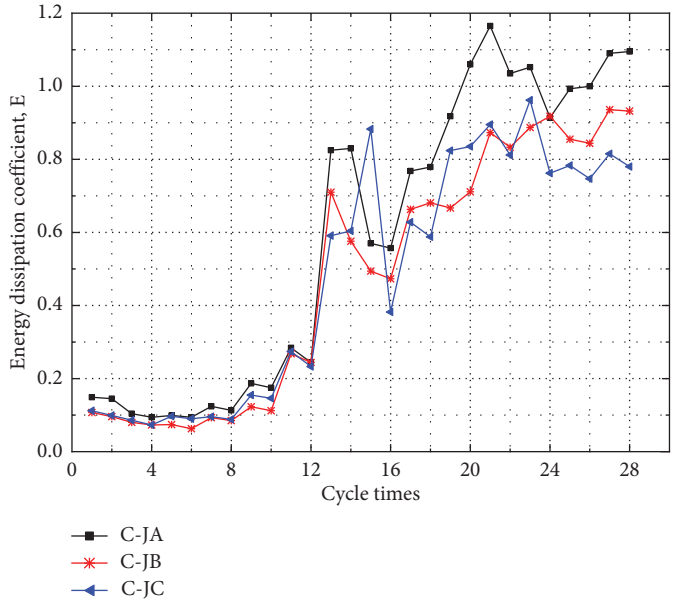

Figure 10: Comparison of the energy dissipation coefficient.

2.3.4. Failure Mode. It can be concluded from the test process in Section 2.2 that the plasticity development sequence of the prefabricated semirigid steel frame with X-shaped braces was as follows: the long penetrating brace had a crack parallel to the weld at the connection; with the increase of the stress, the crack gradually penetrated the metal and the brace then broke. The end of the floor-two beam then became unstable, and a plastic hinge effect occurred, and finally a plastic hinge was formed at the bottom of the floor-one column. It basically followed the failure sequence of brace-beam-column. The structure had two seismic fortification lines, which met the design requirements of "strong column and weak beam" and "strong connection and weak component."

3. Verification by Finite Element Analysis

3.1. Building of the Model. The FEM models were built by the finite element platform of ABAQUS software. As we all know, the shell element could effectively reduce the computing time with the same calculation accuracy, so the general shell element S4R was selected to simulate the steel frame and braces because of its steady performance and extensive scope of application. The spring unit SPRING2 was used to simulate the semirigid connections. According to the previous data for connection analysis, the nonlinear connection characteristics were given by modifying the INP file. The model adopted a bilinear isotropic kinematic hardening model, obeyed the Mises yield criterion, the relevant flow criterion and the kinematic hardening criterion. The Bauschinger effect was considered and Poisson's ratio was 0.3. Swept meshing was conducted to get the hexahedral elements and the mesh size was 1/20. The plasticity data and elastic modulus of the steel could be obtained in Table 3. The finite element model is shown in Figure 11.

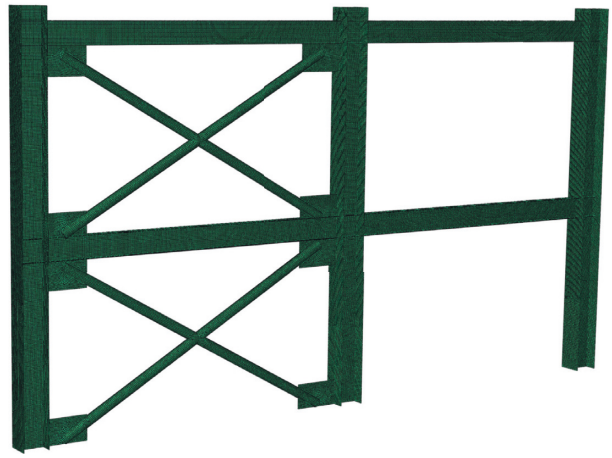

Figure 11: FEM model.

3.2. Hysteresis Curve. The hysteresis curves of the test results and the FEM analysis result are shown in Figure 12.

It can be seen from Figure 12 that the hysteresis curve obtained by the finite element analysis agreed well with that obtained from the test, and the errors between the two methods in terms of yield load, peak load and ultimate load were within 10%, indicating that the ABAQUS model can simulate the mechanical properties of the specimen satisfactorily. However, there were still some differences between the two methods and the reasons are as follows:

(1) Compared with the test results, the hysteresis curves obtained by the finite element analysis were fuller, the area enclosed by the hysteresis loop was larger, and there was no pinching phenomenon. This was because the bolt connecting the actuator and the specimen became loose in the middle and final stages of the test. Therefore, a slipping phenomenon occurred during the process of reciprocating loading,

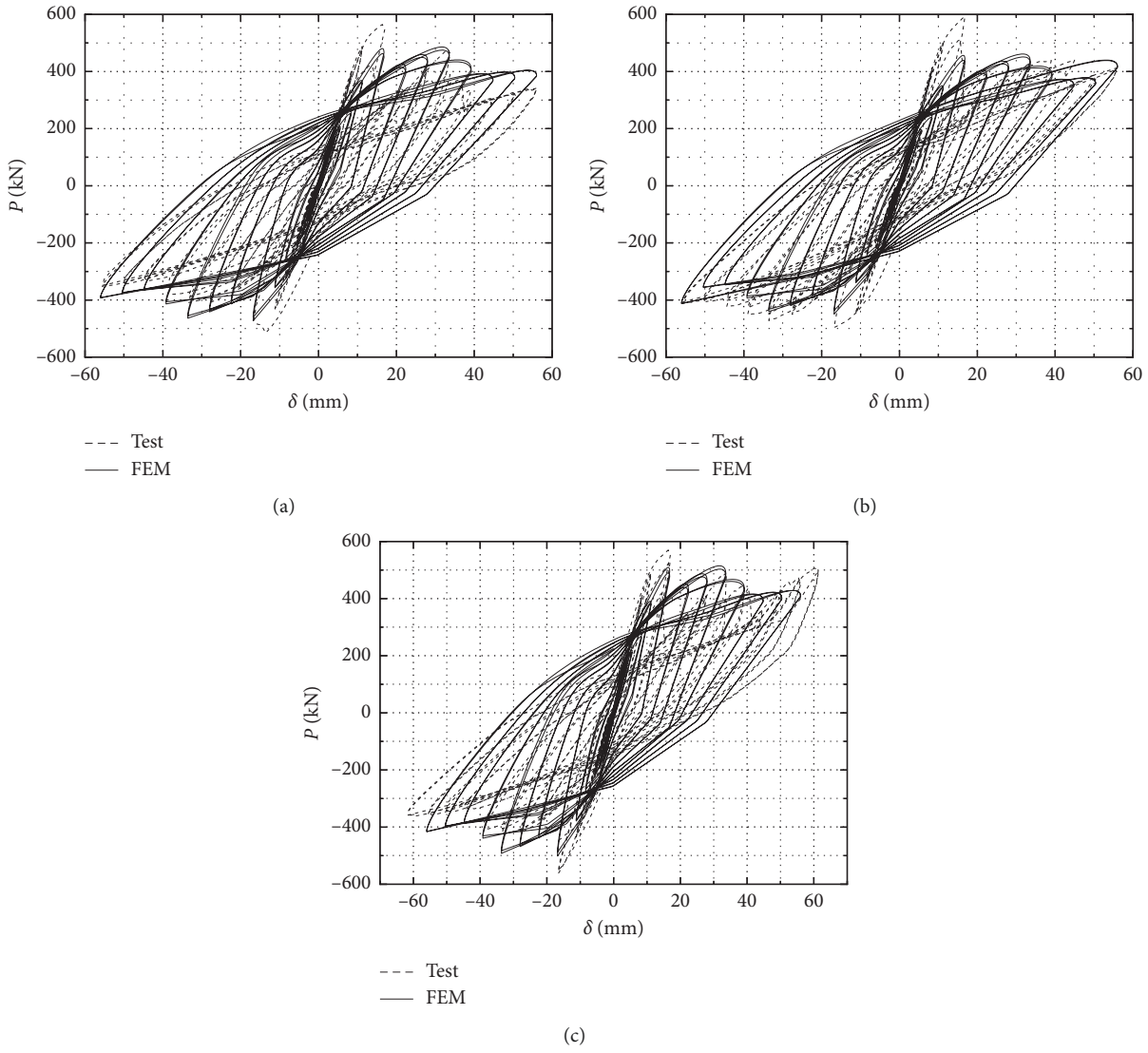

Figure 12: Hysteresis curve comparison of the specimens. (a) Hysteresis curve comparison of the specimen C-JA. (b) Hysteresis curve comparison of the specimen C-JB. (c) Hysteresis curve comparison of the specimen C-JC.

resulting in a certain pinch in the test results. However, this phenomenon did not occur in the finite element analysis.

(2) The load-bearing capacity in the final stage of the finite element analysis was higher than the test value. This was because there were initial defects in the actual material, which will have a certain influence on the test results, while the initial defects of the material were not considered in the finite element analysis.

3.3. Load Bearing Capacity. The yield stress and yield displacement of the specimen were determined by using the general yield bending moment method [32], as shown in Figure 13. Points A, B, C, and D represent the initial yield point, yield point, peak load point, and failure load point of the specimen, respectively. Among them, according to the Specification for seismic test of buildings [31], there are

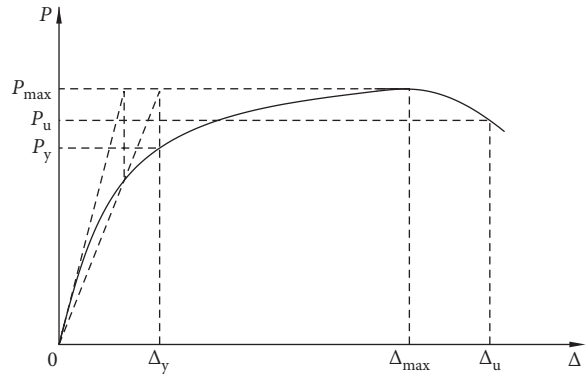

Figure 13: General yield bending moment method.

$P_u = 0.85P_{max}$ and the corresponding Δ_u represents the limit displacement of the specimen. The ductility of the structure is measured by the displacement ductility factor

Table 5: Comparison of the finite element analysis and experimental results of specimen C-JA.

Items	P_y (kN)	Δ_y (mm)	P_{max} (kN)	Δ_{max} (mm)	P_u (kN)	Δ_u (mm)
Test result	485	15.2	489	17.3	416	24.3
ABAQUS result	449	14.7	463	16.4	394	25.6
Error (%)	7.4	3.3	5.3	5.2	5.3	5.1

Table 6: Comparison of the finite element analysis and experimental results of specimen C-JB.

Items	P_y (kN)	Δ_y (mm)	P_{max} (kN)	Δ_{max} (mm)	P_u (kN)	Δ_u (mm)
Test result	479	14.9	506	16.1	430	26.6
ABAQUS result	465	14.1	474	15.4	403	27.9
Error (%)	2.9	5.4	6.3	4.3	6.3	4.9

Table 7: Comparison of the finite element analysis and experimental results of specimen C-JC.

Items	P_y (kN)	Δ_y (mm)	P_{max} (kN)	Δ_{max} (mm)	P_u (kN)	Δ_u (mm)
Test result	507	15.4	535	17.0	455	28.2
ABAQUS result	479	14.5	508	15.8	432	31.6
Error (%)	5.5	5.8	5.0	7.1	5.0	12.1

Note. The error is the ratio of the difference between the test result and the FEM result to the test result.

μ, which is the ratio of the ultimate displacement Δ_u to the yield displacement Δ_y, i.e.:

$$\mu = \frac{\Delta_u}{\Delta_y}. \quad (2)$$

The comparison of the bearing capacity between the finite element analysis and test are shown in Tables 5–7. It can be seen from the tables that the ABAQUS model could accurately predict the yield load, peak load and ultimate load of the specimen and the error was within 8%. The error in the yield displacement did not exceed 5.8%, but the limit displacement error of C-JC was relatively large. The main reason is that the connection was always in a multi-directional stress state during the test, and the load-bearing capacity was suddenly reduced due to fatigue failure. In contrast, the plasticity in the finite element analysis was continuously accumulated, with no brittle fracture, so the load bearing capacity was not significantly reduced and a large error was generated.

According to equation (2), the ductility coefficient was calculated to be 1.7–2.2, and the ductility was acceptable. If the connection was strengthened or connected in a stronger way, the brace could be prevented from prematurely breaking during the test process, and the ductility performance could also be effectively improved. The stiffness calculated by the finite element analysis was slightly higher than that produced by the test. It can be seen that the existence of the initial defects in the steel caused part of components to enter the yielding stage too early, which reduced the initial stiffness of the structure. However, the influence of the material's initial defects was not considered in the ABAQUS model.

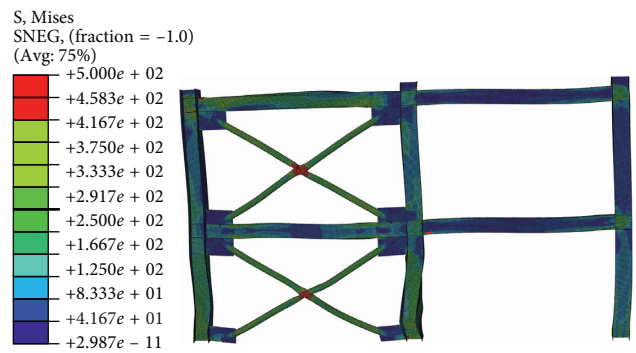

Figure 14: Stress program of the specimens.

3.4. Stress Analysis. Due to the limited space in this paper, only the von Mises stress cloud of the specimen C-JB is presented in Figure 14. It can be seen from Figure 14 that when the specimen reached the limit state, a large plastic deformation occurred at the connection, and the brace broke and did not function, as shown in Figures 15 and 16. The beam end (as shown in Figure 17) and the column foot entered the plastic stage and produced plastic hinges, but they still had load-bearing capacity. Through the analysis, it could be found that under the action of horizontal load, the braces yielded first and dissipated the energy. Therefore, this can reduce the stress on the columns and beams, effectively protecting the main load-bearing components, preventing the sudden collapse of the structure in a large earthquake, and meeting the requirements of multi seismic fortification lines.

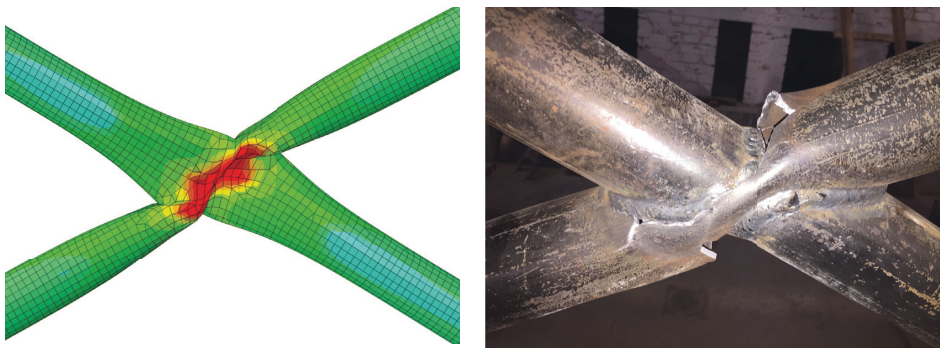

(a) (b)

Figure 15: Failure of the brace's cross joint (first floor). (a) FEM result. (b) Test phenomenon.

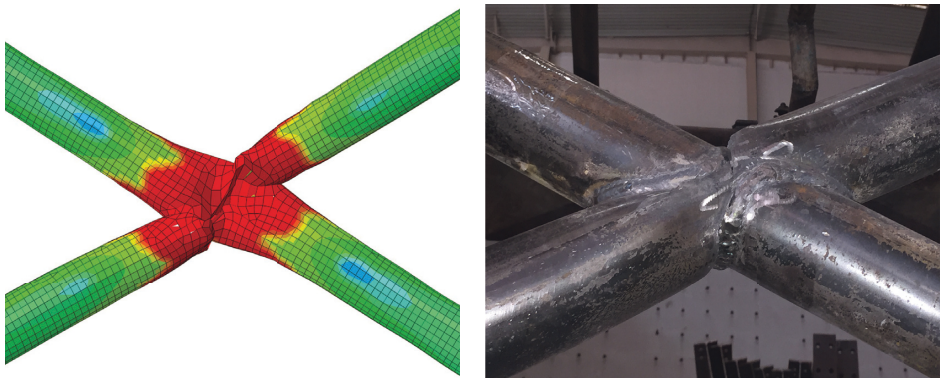

(a) (b)

Figure 16: Failure of the brace's cross joint (second floor). (a) FEM result. (b) Test phenomenon.

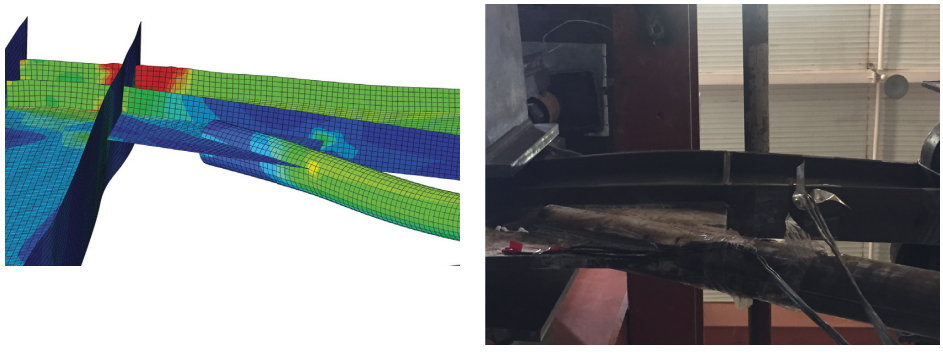

(a) (b)

Figure 17: Plastic hinge of the beam end (second floor). (a) FEM result. (b) Test phenomenon.

4. Conclusions

In this paper, three different semirigid connections between beams and columns were proposed, and the quasi-static test and finite element analysis were performed on the prefabricated semirigid steel frame with X-shaped braces. The following conclusions have been made:

(1) The prefabricated semirigid steel frame with X-shaped braces showed excellent seismic performance, a full hysteresis curve, strong energy dissipation capacity, and relatively stable load-bearing capacity under a large deformation state.

(2) Compared with the top-seat angle connection with web and ear plates, and the T-section connection, the semirigid steel frame with X-shaped braces exhibited excellent load bearing capacity and ductility when the extended end-plate bolted connection was

adopted, and the connections were easy to produce and install, with reasonable paths for stress transmission. This form should be selected in preference.

(3) In the prefabricated semirigid steel frame-with X-shaped braces, the braces failed before the steel frame failed, and the braces and the steel frame had good coordination. The system had two seismic fortification lines with a level of high safety.

(4) The results of the finite element analysis were basically consistent with the test results, indicating that the finite element model established in this paper could accurately simulate the mechanical behavior of a semirigid steel frame with X-shaped braces under reciprocating load.

5. Future Direction

Although the seismic response of the prefabricated semirigid steel frame with X-shaped braces and three different semirigid connections has been preliminarily studied, more analytical data are still required to further examine this structural system. As the behavior of connections can be significantly affected by various connection types and the number of bolts, more finite element studies will be conducted to investigate the behavior patterns of different connections. This will facilitate further evaluation of the rotational stiffness of beam-column connections and their influences on the seismic performance of the structure. Furthermore, different brace arrangements and sections will be studied to optimize the performance of this type of structural system.

Data Availability

The data used to support the findings of this study are available from the corresponding author upon request.

Conflicts of Interest

The authors declare that they have no conflicts of interest.

Acknowledgments

This paper was supported by Scientific Research and Development Project for Wall Material Innovation and Building Energy-Saving of Shandong Province of China (Lucaijianzhi (2014) 139).

References

[1] J. P. Hao, X. Sun, Q. Xue et al., "Research and applications of prefabricated steel structure building systems," *Engineering Mechanics*, vol. 34, no. 1, pp. 1–13, 2017.

[2] J. Wang, J. Zhao, and Z. Hu, "Review and thinking on development of building industrialization in China," *China Civil Engineering Journal*, vol. 49, no. 5, pp. 1–8, 2016.

[3] B. Guo, G. Liu, C. Xu et al., "Experimental study on dynamic characteristic and seismic performance of semi-rigid steel frame with eccentric brace," *Journal of Building Structures*, vol. 32, no. 10, pp. 90–96, 2011.

[4] S. L. Chan and P. P. T. Chui, *Non-Linear Static and Cyclic Analysis of Steel Frames with Semi-Rigid Connections*, Elsevier, London, UK, 2000.

[5] J. C. Ermopoulos, "Buckling length of framed compression members with semirigid connections," *Journal of Constructional Steel Research*, vol. 18, no. 2, pp. 139–154, 1991.

[6] M. S. Ghobadi and R. Ahmady Jazany, "Seismic demand assessment of code-designed continuity plate in panel zone," *Bulletin of Earthquake Engineering*, vol. 17, no. 2, pp. 891–926, 2018.

[7] E. D'Alessandro, G. De Matteis, and G. Brando, "Design charts for end-plate beam-to-column steel joints," *Proceedings of the Institution of Civil Engineers: Structures and Buildings*, vol. 171, no. 6, pp. 472–486, 2018.

[8] Y. Shi, M. Wang, Y. Wang, Y. Wen, and G. Shi, "Rehabilitation of steel moment connections with cover plates under initial loading," *Advances in Structural Engineering*, vol. 14, no. 5, pp. 789–800, 2011.

[9] R. Ahmady Jazany and M. S. Ghobadi, "Seismic evaluation and upgrading details of plate-reinforced moment-resisting connections," *Journal of Constructional Steel Research*, vol. 150, pp. 230–248, 2018.

[10] G. Brando, G. Sarracco, and G. De Matteis, "Strength of an aluminum column web in tension," *Journal of Structural Engineering (United States)*, vol. 141, no. 7, Article ID 4014180, 2015.

[11] S. M. R. Farooghi Mehr and M. S. Ghobadi, "Seismic performance of retrofitted WFP connections joined to box column using ribs," *Journal of Constructional Steel Research*, vol. 137, pp. 297–310, 2017.

[12] D. Erkan, S. Soner, M. P. Saka, and K. Celalettin, "Investigating the effect of joint behavior on the optimum design of steel frames via hunting search algorithm," *Advanced Steel Construction*, vol. 14, no. 2, pp. 168–183, 2018.

[13] C. Faella, V. Piluso, and G. Rizzano, "Review of structural steel semi-rigid connections: theory, design and software," *Engineering Structures*, vol. 22, no. 11, pp. 1578-1579, 2000.

[14] T. Hagishita and M. Ohsaki, "Optimal placement of braces for steel frames with semi-rigid joints by scatter search," *Computers and Structures*, vol. 86, no. 21-22, pp. 1983–1993, 2008.

[15] M. S. Hayalioglu and S. O. Degertekin, "Minimum cost design of steel frames with semi-rigid connections and column bases via genetic optimization," *Computers and Structures*, vol. 83, no. 21-22, pp. 1849–1863, 2005.

[16] I. G. Raftoyiannis, "The effect of semi-rigid joints and an elastic bracing system on the buckling load of simple rectangular steel frames," *Journal of Constructional Steel Research*, vol. 61, no. 9, pp. 1205–1225, 2005.

[17] Y. Zhang, Z. Wang, W. Zhao et al., "A pseudo-dynamic test study on a self-centering prefabricated steel frame with a column base connected by semi-rigid joints," *Advanced Steel Construction*, vol. 12, no. 3, pp. 295–315, 2016.

[18] Z. Fu, K. Ohi, K. Takanashi, and X. Lin, "Seismic behavior of steel frames with semi-rigid connections and braces," *Journal of Constructional Steel Research*, vol. 46, no. 1–3, pp. 440-441, 1998.

[19] M. Elchalakani, R. Grzebiet, and X.-L. Zhao, "Tests of cold-formed circular tubular braces under cyclic axial loading," *Journal of Structural Engineering*, vol. 129, no. 4, pp. 507–514, 2003.

[20] G. Apostolakis and G. F. Dargush, "Optimal seismic design of moment-resisting steel frames with hysteretic passive devices," *Earthquake Engineering and Structural Dynamics*, vol. 39, no. 4, pp. 355–376, 2010.

[21] T. L. Karavasilis, S. Kerawala, and E. Hale, "Hysteretic model for steel energy dissipation devices and evaluation of a minimal-damage seismic design approach for steel buildings (2012)," *Journal of Constructional Steel Research*, vol. 70, pp. 358–367, 2012.

[22] G. Brando, F. D'Agostino, and G. De Matteis, "Seismic performance of MR frames protected by iscous or hysteretic dampers," *Structural Design of Tall and Special Buildings*, vol. 24, no. 9, pp. 653–671, 2015.

[23] G. De Matteis and G. Brando, "Metal shear panels for seismic protection of buildings: recent findings and perspectives," *Ingegneria Sismica*, vol. 33, no. 3, pp. 5–27, 2016.

[24] J. K. Whittle, M. S. Williams, T. L. Karavasilis, and A. Blakeborough, "A comparison of viscous damper placement methods for improving seismic building design," *Journal of Earthquake Engineering*, vol. 16, no. 4, pp. 540–560, 2012.

[25] L. Shen, J. Tian, and Y. Liu, "Performance-based seismic design of eccentrically braced steel frames using target drift and failure mode," *Earthquakes and Structures*, vol. 13, no. 5, pp. 443–454, 2017.

[26] G. J. O'Reilly, J. Timothy, and T. J. Sullivan, "Fragility functions for eccentrically braced steel frame structures," *Earthquakes and Structures*, vol. 10, no. 2, pp. 367–388, 2016.

[27] Y. Wang and G. Dai, *Examples of Seismic Design Specification of Buildings*, China Building and Building Press, Beijing, China, 2006.

[28] GB 50011-2010, *Code for Seismic Design of Building*, China Architecture and Building Press, Beijing, China, 2010.

[29] GB/T 228.1-2010, *Metallic Materials: Tensile Testing: Part 1: Method of Test at Room Temperature*, China Standard Press, Beijing, China, 2011.

[30] GB/T 2975-1998, *Steel and Steel Products—Location and Preparation of Specimens for Mechanical Testing*, China Standard Press, Beijing, China, 1999.

[31] JGJ/T 101-2015, *Specification for Seismic Test of Buildings*, China Architecture & Building Press, Beijing, China, 2015.

[32] B. Zhu, *Seismic Test of Structures*, Seismological Press, Beijing, China, 1989.

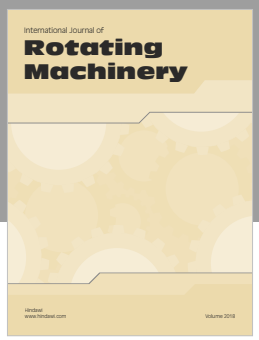

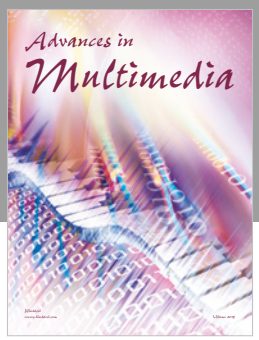

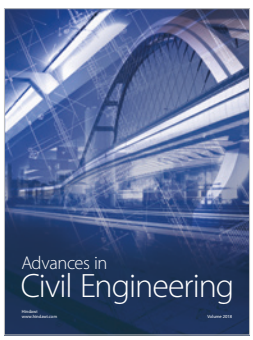

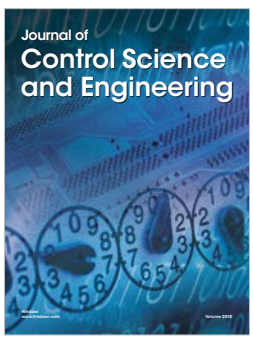

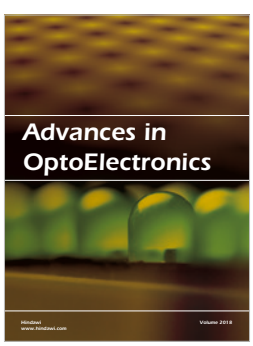

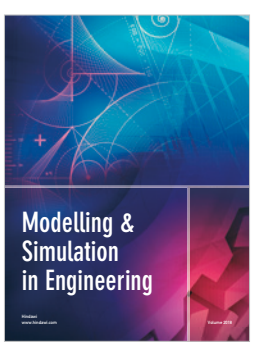

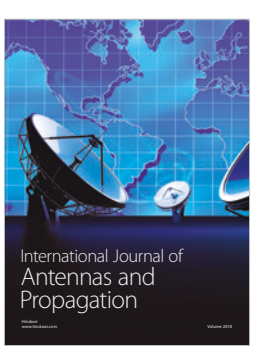

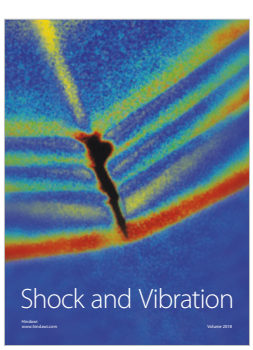

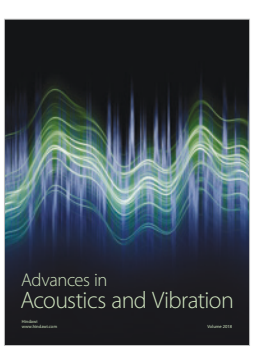

Hindawi

Submit your manuscripts at
www.hindawi.com